Pramana **97**, 2 (2023) [DOI: 10.1007/s12043-022-02480-2]

Galaxy rotation curves in superfluid vacuum theory

Konstantin G. Zloshchastiev*
Institute of Systems Science, Durban University of Technology, P.O. Box 1334, Durban, 4000, South Africa
E-mail: kostiantynz@dut.ac.za, kostya@u.nus.edu
(Dated: received: 24 Feb 2022)

Logarithmic superfluid theory of physical vacuum suggests that gravity has a multiple-scale structure; where one can recognize sub-Newtonian, Newtonian, logarithmic, linear and quadratic (de Sitter) terms in the induced spacetime metric and effective potential. To test the theory's predictions on a galactic scale, we apply best-fitting procedures to the rotation curve data obtained from fifteen galaxies by the HI Nearby Galaxy Survey; assuming their stellar disk's parameters to be fixed to the mean values measured using photometric methods. Although the fitting results seem to be sensitive to a stellar disk model chosen, they correspond closely with observational data, even for those galaxies which rotation velocity profiles do not have flat regions.

PACS numbers: 98.62.Dm, 04.60.Bc, 95.35.+d, 95.36.+x
Keywords: modified gravity; extragalactic astrophysics; quantum gravity; superfluid vacuum; galaxy rotation curve; kinematics and dynamics of galaxies; photometry of galaxies

1. INTRODUCTION

According to Newtonian gravity, the rotation velocity of non-relativistic bodies is inversely proportional to the square root of the distance from a gravitating center, thus resulting in Keplerian orbits. This theory is expected to be applicable to rotating stars and gas in galaxies, especially far from galactic cores where relativistic effects become negligible. However, multiple observations of rotation velocities of stars around the centers of galaxies reveal tremendous discrepancies from Keplerian behaviour. These grow as one proceeds from the inner galactic regions to the furthest data points. The observed data shows rather diverse behaviour of rotation curves, often including, but not restricted to, flat rotation curve (FRC) regimes in the outer regions. Generally, there are two most popular ways of addressing this problem.

The most direct way is that there is a large amount of non-luminous matter, dubbed dark matter (DM), which interacts with luminous matter only through gravity. However, after decades of research, no direct evidence of the existence of dark matter particles has been found. Besides, Standard Model of particle physics and related experiments have placed rather strict bounds upon exotic particles' existence and properties. This inspires further theoretical studies in search of other explanations for the discrepancy between luminous matter's gravitating potential and its observed one.

There is also a growing understanding that a convincing theory of DM-attributed phenomena cannot be a stand-alone or purely phenomenological model; but should, instead, be rooted in an axiomatic fundamental theory involving all known interactions. It is also agreed that creating this fundamental theory would not be possible without a clear picture of what the physical vacuum - a natural phenomenon which underlies all known particles and interactions - is all about.

One of the simplest and physically clear candidates for a theory of physical vacuum and quantum gravity is superfluid vacuum theory (SVT). This framework has foundations in Dirac's idea of the physical vacuum being a nontrivial object described by quantum wavefunction [1]. Since his work, various approaches have been proposed, which agree on the main paradigm (of physical vacuum being a background quantum liquid and elementary particles being excitations thereof [2, 3]), but which vary in details. In this paper, we will be using a modern version of the superfluid vacuum approach, logarithmic superfluid vacuum theory; its details can be found in the landmark papers [4–6].

The paper is organized as follows. Theory of physical vacuum based on the logarithmic superfluid model is outlined in Sec. 2, including the derivation of effective gravitational potential induced by the superfluid vacuum in a given quantum state. Galaxy rotation curves and their best fit results based on the logarithmic superfluid vacuum theory are presented in Sec. 3. Discussion of results and conclusions are presented in sections 4 and 5, respectively.

2. INDUCED SPACETIME AND EFFECTIVE GRAVITY

In this section, closely following the lines of the work [6], we derive the effective gravitational potential of the logarithmic superfluid vacuum in the presence of a large density inhomogeneity, serving as a gravitating center and reference point.

The theory assumes that the physical vacuum is described, when disregarding quantum fluctuations, by the fluid wavefunction $\Psi(\boldsymbol{r}, t)$, which is a three-dimensional Euclidean scalar. The quantum state of the fluid itself is described by a ray in the corresponding Hilbert space,

*Electronic address: https://bit.do/kgz

therefore, this wavefunction obeys the normalization condition $\langle\Psi|\Psi\rangle = \int_{\mathcal{V}} \rho\, d\mathcal{V} = \mathcal{M}$, where $\mathcal{M}$ and $\mathcal{V}$ are the total mass and volume of the fluid, respectively, and $\rho = |\Psi|^2$ is the fluid mass density. The wavefunction's evolution is governed by a wave equation of a Schrödinger type but with logarithmic nonlinearity:

$$i\hbar\partial_t\Psi = \left[-\frac{\hbar^2}{2m}\boldsymbol{\nabla}^2 + V_{\rm ext}(\boldsymbol{r},t) - \Big(b_0 - \frac{q}{r^2}\Big)\ln\Big(\frac{|\Psi|^2}{\bar\rho}\Big)\right]\Psi, \tag{1}$$

where m is the constituent particles' mass, $V_{\rm ext}(\boldsymbol{r},t)$ is an external or trapping potential (to be neglected for simplicity in what follows), $r = |\boldsymbol{r}| = \sqrt{\boldsymbol{r}\cdot\boldsymbol{r}}$ is a radius-vector's absolute value, and b_0 and q are real-valued constants. Despite its resemblance to Schrödinger equations, eq. (1) should not be confused with theories of nonlinear quantum mechanics [7]. Instead, the logarithmic nonlinearity is induced by many-body effects in the quantum Bose liquid, whereas the underlying quantum mechanics remains conventional.

In this picture, massless excitations, such as photons, are somewhat analogous to acoustic waves propagating with velocity $c_s \propto \sqrt{p'(\rho)}$, where fluid pressure is determined via the equation of state $p = p(\rho)$, and the prime denotes a derivative with respect to the argument in brackets. A relativistic observer "sees" himself located inside four-dimensional curved spacetime with a pseudo-Riemannian metric:

$$g_{\mu\nu} \propto \frac{\rho}{c_s}\begin{pmatrix} -\left[c_s^2 - \eta^2(\boldsymbol{\nabla}S)^2\right] & \vdots & -\eta\boldsymbol{\nabla}S \\ \cdots\cdots & \cdot & \cdots \\ -\eta\boldsymbol{\nabla}S & \vdots & \mathbf{I} \end{pmatrix}, \tag{2}$$

where $\eta = \hbar/m$, $S = S(\boldsymbol{r},\,t) = -i\ln\left(\Psi(\boldsymbol{r},\,t)/|\Psi(\boldsymbol{r},\,t)|\right)$ is a phase of the condensate wavefunction written in the Madelung representation, $\Psi = \sqrt{\rho}\exp(iS)$, and $\mathbf{I}$ is a three-dimensional unit matrix. In this picture, Einstein field equations are interpreted as a definition for an induced stress-energy tensor, describing some effective matter, as observed by a relativistic observer, $\widetilde{T}_{\mu\nu} \equiv \kappa^{-1}\left[R_{\mu\nu}(g) - \frac{1}{2}g_{\mu\nu}R(g)\right]$, where $\kappa = 8\pi G/c_{(0)}^2$ is the Einstein's gravitational constant, G is the Newton's gravitational constant, and $c_{(0)} \approx c$, where $c = 2.9979\times10^{10}$ $\mathrm{cm\,s^{-1}}$ is historically called the *speed of light in vacuum.*

If the physical vacuum is in a quantum state described by wavefunction $\Psi = \Psi_{\rm vac}(\boldsymbol{r},\,t)$, then the solution of eq. (1) is equivalent to the solution of the linear Schrödinger equation with effective potential, which can be written (in Cartesian coordinates) as:

$$\Phi = -\frac{1}{m}V_{\rm eff}(\boldsymbol{r},t) = \frac{1}{m}\left(b_0 - \frac{q}{r^2}\right)\ln\left(\frac{|\Psi_{\rm vac}(\boldsymbol{r},t)|^2}{\bar\rho}\right), \tag{3}$$

where we disregard any anisotropy and rotation.

According to logarithmic SVT, Lorentz symmetry emerges in the "phononic" (low-momentum) limit, where SVT can be well approximated by the theory of general relativity [8, 9]. Correspondingly, a relativistic observer would perceive gravity induced by the potential (3) as curved four-dimensional spacetime. In a rotationally invariant case, the line element of such spacetime can be written as

$$\begin{aligned} ds^2 &= -K^2c_{(0)}^2dt^2 + \frac{1}{K^2}dr^2 + R^2(r)d\sigma^2, \\ K^2 &\equiv 1 + 2\Phi/c_{(0)}^2, \end{aligned} \tag{4}$$

where $R(r) = r\left[1 + \mathcal{O}\left(\Phi/c_{(0)}^2\right)\right] \approx r$, $d\sigma^2 = d\theta^2 + \sin^2\theta\, d\varphi^2$ is the line element of a unit two-sphere.

Furthermore, because we do not know the exact wavefunction of the physical vacuum, we must resort to general arguments and trial functions whose parameters are to be determined empirically. We expect that our vacuum is currently in a stable state, which is close to a ground state or at least to a metastable state, with a sufficiently large lifetime. It is thus natural to assume that the state $|\Psi_{\rm vac}\rangle$ is stationary and rotationally invariant, and use the following ansatz for its amplitude:

$$|\Psi_{\rm vac}| = \sqrt{\bar\rho}\,\left(\frac{r}{\bar\ell}\right)^{\chi/2} P\,(r)\,\exp\Big(-\frac{a_2}{2}r^2 + \frac{a_1}{2}r + \frac{a_0}{2}\Big), \tag{5}$$

where $P(r)$ is a polynomial function, χ and a's are constant parameters of the solution. Here $\bar\ell$ is the length scale of the logarithmic nonlinearity – which can be chosen to be the classical length $(m/\bar\rho)^{1/3}$ or the quantum temperature length $\hbar/\sqrt{mb_0}$. For reasons explained in [6], these constants' values remain theoretically unknown at this stage. From the empirical point of view, the function (5) can be considered a trial function, whose parameters can be fixed using experimental data.

By substituting the trial solution (5) into the definition (3), we derive the effective gravitational potential

$$\begin{aligned} \Phi &= \Phi_{\rm smi}(r) + \Phi_{\rm RN}(r) + \Phi_{\rm N}(r) \\ &\quad + \Phi_{\rm (ln)}(r) + \Phi_{(1)}(r) + \Phi_{(2)}(r) + \Phi_0, \end{aligned} \tag{6}$$

where $\Phi_0 = (a_0b_0 + a_2q)/m$ is the additive constant,

$$\Phi_{\rm smi}(r) = -\frac{q}{mr^2}\ln\left[\left(\frac{r}{\bar\ell}\right)^{\chi}P^2(r)\right], \tag{7}$$

$$\Phi_{\rm RN}(r) = -\frac{a_0\,q}{m}\frac{1}{r^2}, \tag{8}$$

$$\Phi_{\rm N}(r) = -\frac{a_1q}{m}\frac{1}{r} = -\frac{GM}{r}, \tag{9}$$

$$\Phi_{\rm (ln)}(r) = \frac{b_0}{m}\ln\left[\left(\frac{r}{\bar\ell}\right)^{\chi}P^2(r)\right], \tag{10}$$

$$\Phi_{(1)}(r) = \frac{a_1b_0}{m}r, \tag{11}$$

$$\Phi_{(2)}(r) = -\frac{a_2b_0}{m}r^2, \tag{12}$$

where M is the (induced) gravitational mass of the configuration.

The main simplifying assumptions and approximations underlying the derivation of the potential are summarized in the Appendix B of [6]. Note also that in

the work [6] we used a simple approximate form of the non-exponential part of the wavefunction amplitude, $\left(r/\bar{\ell}\right)^{\chi/2} P\left(r/\bar{\ell}\right) \approx \left(r/\bar{\ell}\right)^{\chi/2}$, which resulted in a simplified form of logarithmic terms in the effective potential and induced spacetime metric. That approximation was sufficient for the illustrative purpose of explaining the FRC regime, and was also robust for asymptotic studies of rotation curves in [10]; but for the purposes of this paper it is prudent to do not specify $P(r)$ in formula (5) until the next section.

Last but not least, it is important to emphasize the meaning of the term 'effective potential' here. From the construction of eq. (3), it is clear that no potential exists in reality – instead, many-body quantum-mechanical effects in the supefluid act in the manner we perceive as gravitational potential. One can imagine a (distant) classical analogy of this process: during the diffusion process of a substance, its individual molecules move from a region of higher concentration to a region of lower concentration, as if they were driven by some macroscopic potential. In our case, the logarithmic term is directly related to the Everett-Hirschman information entropy of the logarithmic superfluid, cf. Section 3 of [6], therefore, it is this entropy's evolution which induces "thermodynamic" force and associated "potential".

3. ROTATION CURVES

From this section onwards, we will work in units $G = 1$. In a spherically symmetric case, the rotation velocity of stars orbiting with non-relativistic velocities on a plane driven by gravitational potential (6), or, alternatively, along geodesics in the induced spacetime (4), can be computed using a simple formula $v^2 = \frac{1}{2} r \frac{d}{dr}(c^2_{(0)} K^2)\big|_{r=R} = R\,\Phi'(R)$, where v is the orbital velocity and R is the orbit's radius. We assume that this formula is approximately valid in the cylindrically symmetric case, which is a common assumption for studies of this kind.

Besides, we will neglect those terms in eq. (6) which decay faster than the Newtonian term at spatial infinity. We thus obtain

$$\Phi(r) = \Phi_{\rm N}(r) + \Phi_{(\ln)}(r) + \Phi_{(1)}(r) + \Phi_{(2)}(r), \qquad (13)$$

where the additive constant is omitted as well. Using this truncated potential, we obtain

$$v(R) \;=\; \left\{ R\frac{d}{dR}\left[\Phi_{\rm N}(R) + \Phi_{(\ln)}(R) + \Phi_{(1)}(R) + \Phi_{(2)}(R)\right]\right\}^{1/2} = \sqrt{v^2_{\rm N} + v^2_{(\ln)} + \tilde{a}_1 R - \tilde{a}_2 R^2}, \qquad (14)$$

where

$$v^2_{(\ln)} \;=\; \frac{b_0}{m} R\,\frac{d}{dR}\ln\left[\left(\frac{R}{\bar{\ell}}\right)^{\chi} P^2(r)\right] = \frac{b_0}{m} R\,\frac{d}{dR}\left\{\chi \ln\left(\frac{R}{\bar{\ell}}\right) + \ln\left[P^2(r)\right]\right\}, \qquad (15)$$

where the tilde denotes the multiplication by b_0/m (such as $\tilde{a}_1 = (b_0/m)a_1$ et cetera), and $v_{\rm N}$ is the rotation velocity derived from Newtonian dynamics.

As mentioned in the previous section, an exact form of the polynomial $P(x)$ is not yet theoretically known. In the works [6, 10], we used the approximation $P(r) \approx r$, which was sufficient for our purposes there. In this paper, we assume a slightly more general form

$$P(r) \approx k_2 r^2 + k_1 r + 1, \qquad (16)$$

therefore

$$v^2_{(\ln)} \approx \frac{b_0}{m} R\,\frac{d}{dR}\left\{\chi \ln\left(\frac{R}{\bar{\ell}}\right) + \ln\left[\left(k_2 R^2 + k_1 R + 1\right)^2\right]\right\}, \qquad (17)$$

hence

$$v(R) \approx \sqrt{v^2_{\rm N} + \frac{b_0}{m} R\,\frac{d}{dR}\left\{\chi \ln\left(\frac{R}{\bar{\ell}}\right) + \ln\left[\left(k_2 R^2 + k_1 R + 1\right)^2\right]\right\} + \tilde{a}_1 R - \tilde{a}_2 R^2}, \qquad (18)$$

where the coefficients k_i will also have their values fixed according to the best-fitting criteria.

Furthermore, to calculate the velocity $v_{\rm N}$, the mass distribution of a galaxy must be assumed, usually derived from the photometric data. This generally contains two components: gas (mainly neutral hydrogen and helium, any other gases are negligible compared to them) and the stellar disk, while the mass of the bulge is usually neglected for simplicity [11]. Also for a sake of simplicity, it is assumed that both gas and stellar disks are thin.

Name	D	R_d	R_d	M_d	M_d	b_0/m	χ	k_1	k_2	$\tilde{a}_1$	$\tilde{a}_2$
(1)	(2)	(3)	(4)	(5)	(6)	(7)	(8)	(9)	(10)	(11)	(12)
DDO 154	4.3	0.72	0.54	0.00263	0.00186	21.4^2	0	0	0.233	0	4.12×10^{-36}
NGC 925	9.2	3.30	n/a	1.02	0.72	326^2	0.012	0	0.00174	-4.34	2.27×10^{-31}
NGC 2403	3.2	1.81	2.05	0.47	0.33	111.5^2	0	0.171	0	-0.527	3.13×10^{-50}
NGC 2841	14.1	4.22	3.55	10.96	7.59	144^2	0.050	0	0.089	-2.39	5.14×10^{-50}
NGC 2903	8.9	2.40	2.81	1.41	1.0	91.9^2	0	0	0.18	0	3.42×10^{-33}
NGC 2976	3.6	0.91	n/a	0.178	0.126	111.4^2	0	0	0.039	0	4.44×10^{-31}
NGC 3031	3.6	1.93	n/a	6.92	4.9	100.5^2	0	0	0.056	0	4.88×10^{-32}
NGC 3198	13.8	3.06	3.88	2.82	1.995	68.2^2	0	0	0.017	0	2.85×10^{-34}
NGC 3521	10.7	3.09	2.86	12.3	8.71	189^2	0	0	0.017	-7.03	1.68×10^{-47}
NGC 3621	6.6	2.61	n/a	1.95	1.38	64.8^2	0	0.563	0	1.35	8.05×10^{-50}
NGC 4736	4.7	1.99	n/a	1.86	1.32	230.4^2	0.83	0	0.008	-43.8	7.76×10^{-49}
NGC 5055	10.1	3.68	5.00	12.3	8.71	47.6^2	0	80.2	0	1.27	3.06×10^{-51}
NGC 6946	5.9	2.97	n/a	5.89	4.17	165^2	0	0.0543	0	0	1.72×10^{-46}
NGC 7331	14.7	2.41	4.48	16.6	11.7	311^2	0	0	0.0015	-20.1	1.25×10^{-49}
NGC 7793	3.9	1.25	n/a	0.275	0.195	91.6^2	0	0	0.0436	0	1.48×10^{-31}

TABLE I: The best fit of THINGS data, assuming formula (18). Notes: (1) name of galaxy; (2) distance to galaxy, in Mpc; (3) characteristic radius of stellar disk taken from [17], in kpc; (4) characteristic radius of stellar disk taken from [18], in kpc; (5) mass of stellar disk according to the diet-Salpeter IMF, taken from [17], in $10^{10} M_\odot$; (6) mass of stellar disk according to the Kroupa IMF, taken from [17], in $10^{10} M_\odot$; (7) a free parameter, in km^2 s^{-2}; (8) a free parameter, dimensionless; (9) a free parameter, in kpc^{-1}; (10) a free parameter, in kpc^{-2}; (11) a free parameter (related to Rindler acceleration), in 10^{-11} m s^{-2}; (12) a free parameter (related to de Sitter constant), in s^{-2}. Values of free parameters were obtained assuming disk radius and mass from the third and sixth column, respectively.

According to the popular exponential disk model [12], the rotation velocity of stars can be derived as

$$v_\star(R) = c_{(0)} \left\{ \frac{M_d}{2R_d} \left(\frac{R}{R_d} \right)^2 \left[I_0\left(\frac{R}{2R_d} \right) K_0\left(\frac{R}{2R_d} \right) - I_1\left(\frac{R}{2R_d} \right) K_1\left(\frac{R}{2R_d} \right) \right] \right\}^{1/2}, \tag{19}$$

where M_d and R_d are the mass and length scale of the disk, I_n and K_n being the nth-order modified Bessel functions of the first and second kind, respectively.

The Newtonian velocity due to the combined contributions of gas and stellar disk is given by

$$v_{\rm N}(R) = \sqrt{v^2_{\rm gas}(R) + v^2_\star(R)}, \tag{20}$$

where the term $v_{\rm gas}$ takes into account the contributions of both neutral hydrogen and helium.

Furthermore, we perform the best fit to various galaxies data taken from the HI Nearby Galaxy Survey (THINGS) [13, 14]. We use formulae (18)-(20), in which the fitting parameters are going to be b_0/m, χ, k_1, k_2, $\tilde{a}_1$, $\tilde{a}_2$, whereas R_d and M_d are fixed according to an initial mass function model (IMF) chosen [15, 16], as discussed in [17, 18]. The gas contribution $v_{\rm gas}$ can be directly deduced from the database, similar plots can be found in [14, 18]. For simplicity, we use the mean values of the THINGS data.

We make use of the Levenberg–Marquardt least-squares fit method. The results are plotted in figure 1 (cases NGC 7331 and 7793 are being additionally discussed in figures 2 and 3), and corresponding best-fitting parameters are listed in table I. When fitting, we fix the stellar disk radius and mass to the values from its third and sixth column, respectively.

4. DISCUSSION

Before discussing the fitting results themselves, it should be stressed out that there is a large discrepancy in the interpretation of photometric data for stellar disks. Even within the common framework of Freeman's exponential disk model, one gets substantially distinct values

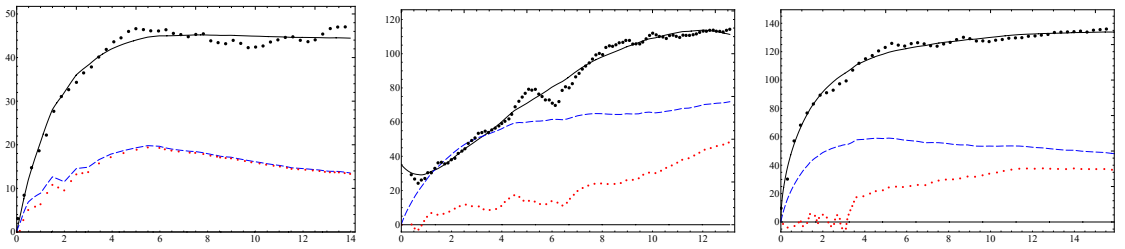

DDO 154 NGC 925 NGC 2403

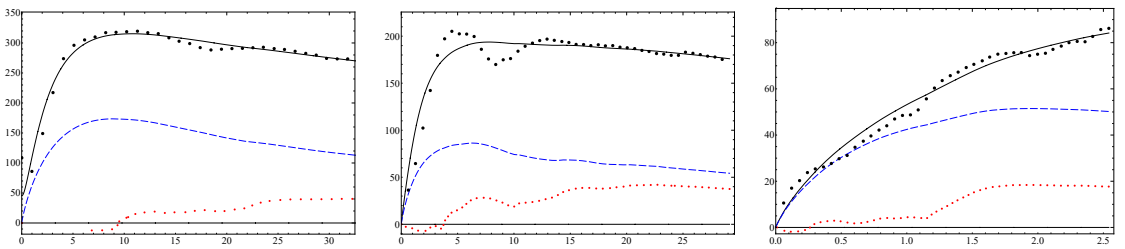

NGC 2841 NGC 2903 NGC 2976

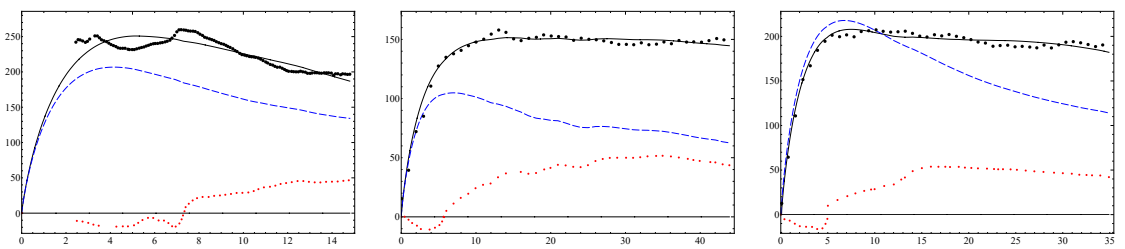

NGC 3031 NGC 3198 NGC 3521

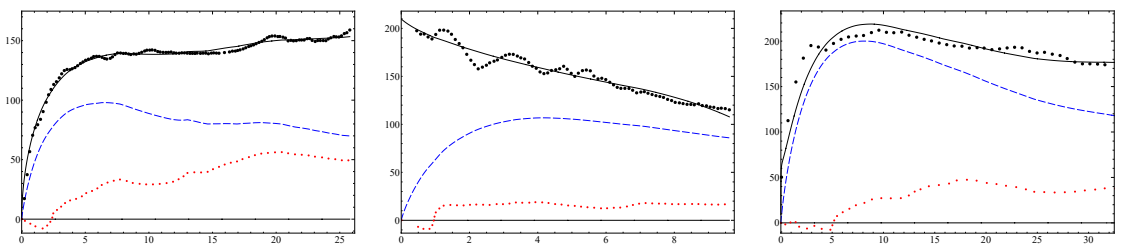

NGC 3621 NGC 4736 NGC 5055

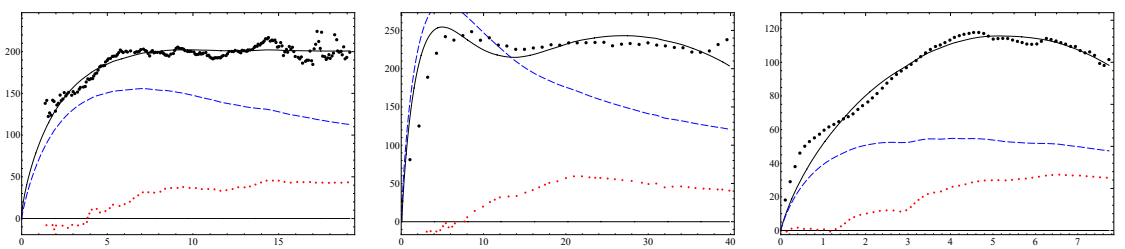

NGC 6946 NGC 7331 NGC 7793

FIG. 1: Least-squares fit (solid curves) to the rotation curves of sample galaxies, for parameters listed in table I. The horizontal axis is the distance R in kpc, and the vertical axis is the rotation velocity in km s^{-1}. Black dots are mean values from the THINGS data, dotted curves are the contribution of gas, dashed curves are the total contribution of gas and stellar disc in Newtonian dynamics. Cases of NGC 7331 and 7793 are separately discussed in figures 2 and 3, respectively.

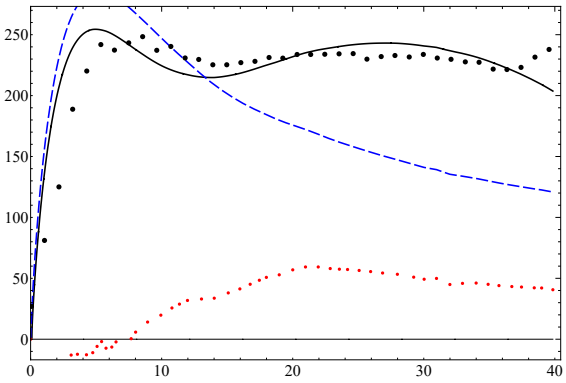

$R_d = 2.41$ kpc

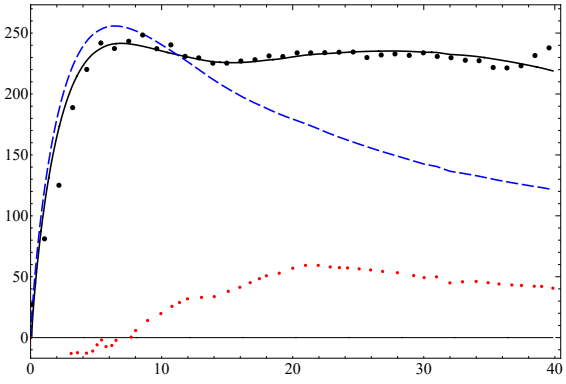

$R_d = 3$ kpc

FIG. 2: NGC 7331: a comparison of fits for different stellar disk parameters. The first panel is the one taken from figure 1, which is based on the fixed parameters from third and sixth column of table I; fitting values of its free parameters are listed therein. The second panel is the best fit based on the disk mass from the same sixth column, but the disk radius being assumed slightly larger; fitting values of the corresponding free parameters are: $b_0/m = 238^2$ km^2 s^{-2}, $\chi = 0$, $k_1 = 0$, $k_2 = 0.00147$ kpc^{-2}, $\tilde{a}_1 = -1.02 \times 10^{-10}$ m s^{-2} and $\tilde{a}_2 = 1.15 \times 10^{-50}$ m s^{-2}. Axes' labels and units are the same as in figure 1.

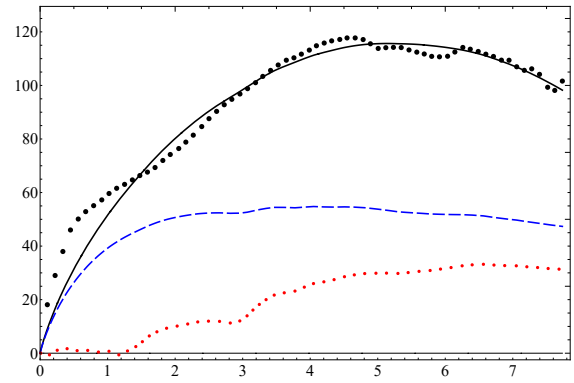

$R_d = 1.25$ kpc

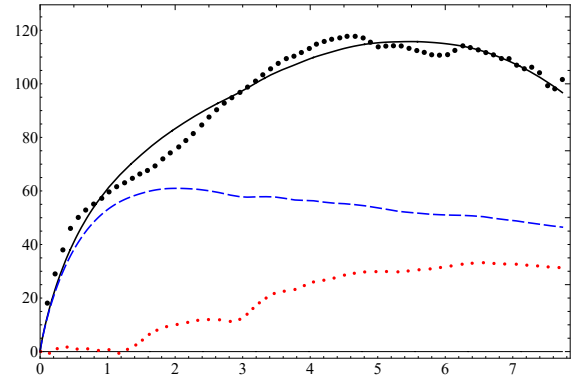

$R_d = 0.9$ kpc

FIG. 3: NGC 7793: a comparison of fits for different stellar disk parameters. The first panel is the one taken from figure 1, which is based on the fixed parameters from third and sixth column of table I; fitting values of its free parameters are listed therein. The second panel is the best fit based on the disk mass from the same sixth column, but the disk radius being assumed slightly smaller; fitting values of the corresponding free parameters are: $b_0/m = 123^2$ km^2 s^{-2}, $\chi = 0$, $k_1 = 0$, $k_2 = 0.0229$ kpc^{-2}, $\tilde{a}_1 = 0$ and $\tilde{a}_2 = 2.44 \times 10^{-31}$ m s^{-2}. Axes' labels and units are the same as in figure 1.

of stellar disk parameters, such as mass and characteristic radii. This uncertainty leads to the increased ambiguity of fitting curves, especially considering the multi-parameter character of the fitting function (18). For these reasons, most of the fitting results are sensitive to the disk models used, see figures 2 and 3 for examples. Yet, a few qualitative features, common for sample galaxies considered can be spotted right away.

To begin with, the power degree χ is responsible for the part of the logarithmic term which diverges at $R \to 0$. This parameter turns out to be zero for most of galaxies, except those whose rotation velocity is not approaching small values at $R \to 0$, such as NGC 925 or 2841. It is not clear however if this occurs due to the lack of precise observational data points at small orbital radii (less than 0.5 kpc).

One immediately notices that the logarithmic coupling b_0/m acquires a large value for all fitting samples. On the other hand, its square root is approximately equal to the average velocity of the galaxy's FRC regime (if a plateau occurs on a curve), or to the peak velocity (if a curve does not have a clearly visible plateau). This suggests that the logarithmic term (10) yields an important, if not predominant, contribution to galactic dynamics for a large range of distances, all the way up to the galactic outskirts. This confirms our earlier result that the logarithmic term is largely responsible for the FRC regime's occurrence the outer regions of galaxies [6], also that it contributes to the crossover from flat to non-flat regimes at galactic outskirts [10].

Furthermore, the linear term seems to affect the shapes

of the rotation curves in middle-to-far regions, but in many cases the fitting result turns out better without assuming this term whatsoever – which may or may not be a consequence of the stellar disk model's uncertainty mentioned above. The quadratic (de Sitter) term contributes to asymptotic behaviour of rotation curves, at the galaxy's border. Despite de Sitter constant's value looking rather small (in sub-astronomical units such as SI or CGS), its presence substantially improves fitting at largest values of the orbital radius.

It seems also that both linear and quadratic terms are unique to each galaxy, which confirms the conjecture of multiple expansion mechanisms, discussed in section 7 of [6]; the galaxy dependence of parameters of effective potentials (therefore, rotation velocities) was discussed in sections 2 and 6 thereof. In essence, nearly all the parameters of the logarithmic superfluid vacuum theory are not the parameters *per se*, but they are dynamical and thermodynamical values. Therefore, they can vary, depending on the environment and boundary conditions: background superfluid not only induces gravitational potential, but also gets affected by it, because this potential acts upon surrounding matter by creating density inhomogeneity.

5. CONCLUSION

In logarithmic superfluid theory, effective gravitational potential is induced by the quantum wavefunction of the physical vacuum of a self-gravitating body or configuration; while the vacuum itself is viewed as the superfluid described by the logarithmic wave equation in the leading-order approximation with respect to Planck constant. Therefore, predicted phenomena are determined not only by original parameters of the model but also shape characteristics of the solution's wavefunction which also depend on boundary conditions. This results in a rich mathematical structure of the theory. For instance, gravity acquires a multiple-scale pattern, to such an extent that one can distinguish the sub-Newtonian, Newtonian, logarithmic, linear (sometimes referred to as Rindler) and quadratic (de Sitter) terms in the effective potential.

Following the lines of our previous works [6, 10], we have applied the best-fitting procedures to the rotation curve data of a number of galaxies from the HI Nearby Galaxy Survey assuming their stellar disk and gas parameters being rigidly fixed to the mean values obtained using photometric methods. Although the fitting results seem to be sensitive to stellar disk models and technical assumptions about the superfluid vacuum's wavefunction, they agree with observational data very well, considering the large range of phenomena involved.

It should be emphasized that successful fitting also takes place for those galaxies whose rotation curves do not have a clearly visible FRC plateau, such as NGC 2976, 4736 and 7793, or have unusual asymptotic behaviour at small values of the orbital radius, such as NGC 925, 2841 and 4736. This is largely possible due to the multi-scale structure of gravity in logarithmic superfluid vacuum theory.

Acknowledgments

Proofreading of the manuscript by P. Stannard is greatly appreciated. This research was funded by Department of Higher Education and Training of South Africa and in part by National Research Foundation of South Africa (Grants Nos. 95965, 131604 and 132202).

[1] P. A. M. Dirac, *Nature* **168**, 906-907 (1951)
[2] G. E. Volovik, *The Universe in a Helium Droplet* (Oxford University Press, Oxford, UK)
[3] K. Huang, *A Superfluid Universe* (World Scientific, Hackensack, NJ, USA)
[4] K. G. Zloshchastiev, *Grav. Cosmol.* **16**, 288-297 (2010)
[5] K. G. Zloshchastiev, *Acta Phys. Polon.* **42**, 261-292 (2011)
[6] K. G. Zloshchastiev, *Universe* **6**, 180 (2020)
[7] I. Bialynicki-Birula and J. Mycielski, *Ann. Phys. (N. Y.)* **100**, 62-93 (1976)
[8] K. G. Zloshchastiev, *Int. J. Mod. Phys. A* **35**, 2040032 (2020)
[9] K. G. Zloshchastiev, *Low Temp. Phys.* **47**, 89-95 (2021)
[10] K. G. Zloshchastiev, *Astron. Rep.* **65**, 1078-1083 (2021)
[11] A. Toomre, *Astrophys. J.* **138**, 385-392 (1963)
[12] K. C. Freeman, *Astrophys. J.* **160**, 811-830 (1970)
[13] F. Walter, E. Brinks, W. J. G. de Blok, F. Bigiel, R. C. Kennicutt Jr., M. D. Thornley and A. Leroy, *Astron. J.* **136**, 2563-2647 (2008)
[14] W. J. G. de Blok, F. Walter, E. Brinks, C. Trachternach, S.-H. Oh and R.C. Kennicutt Jr., *Astron. J.* **136**, 2648-2719 (2008)
[15] E. E. Salpeter, *Astrophys. J.* **121**, 161-167 (1955)
[16] P. Kroupa, *Mon. Not. R. Astron. Soc.* **322**, 231-246 (2001)
[17] J. Mastache, J.L. Cervantes-Cota and A. de la Macorra, *Phys. Rev. D* **87**, 063001 (2013)
[18] H.-N. Lin, M.-H. Li, X. Li and Z. Chang, *Mon. Not. R. Astron. Soc.* **430**, 450-458 (2013)